Comprehensive Modeling and CFD Simulation of Absorption of CO_2 and H_2S by MEA Solution in Hollow Fiber Membrane Reactors

Seyyed Mohammad Hossein Hashemi Amrei, Saber Memardoost, and Asghar Molaei Dehkordi
Dept. of Chemical and Petroleum Engineering, Sharif University of Technology, Tehran, Iran

DOI 10.1002/aic.14286
Published online November 18, 2013 in Wiley Online Library (wileyonlinelibrary.com)

A comprehensive mathematical model has been developed for the simulation of simultaneous chemical absorption of carbon dioxide and hydrogen sulfide by means of Monoethanolamine (MEA) aqueous solution in hollow fiber membrane reactors is described. In this regard, a perfect model considering the entrance regions of momentum, energy, and mass transfers was developed. Computational Fluid Dynamics (CFD) techniques were applied to solve governing equations, and the model predictions were validated against experimental data reported in the literature and excellent agreement was found. Effects of different disturbances on the dynamic behavior of the reactor were investigated. Moreover, effects of various parameters such as wetting fraction, gas and liquid inlet velocities, inlet temperature of the solvent, MEA concentration, and CO_2 and H_2S compositions were carefully studied. It was found that for large values of gas velocity or small values of liquid velocity, the thermal energy equation can play an important role in the model predictions. © 2013 American Institute of Chemical Engineers *AIChE J*, 60: 657–672, 2014

Keywords: CFD simulation, hollow fiber membrane reactor, gas sweetening, transient analysis, transport phenomena, numerical analysis, steady-state response, dynamic behavior

Introduction

The most serious environmental problem in the world is the global warming. The emission of greenhouse gases is the main reason of the global problem, hence, in recent years; the control of greenhouse gases emission has become a worldwide concern. Most of industrial and domestic gas streams contain acid gases such as carbon dioxide and hydrogen sulfide. The former emitted by industrial activities and power plants using fossil fuels forms about 80% of greenhouse gases. On the other hand, H_2S causes toxic and corrosive problems and also is known as the main reason of several environmental problems such as acid rains. Presence of acidic gases in refinery streams as impurities reduces the quality of these gas streams and causes corrosion problems in pipelines. Therefore, the design of effective and economic devices for simultaneous capturing of CO_2 and H_2S from industrial gas streams is of great importance. Generally, conventional devices for acid gases capturing are based on the gas removal by means of various solvents such as amine based solvents in various reactor configurations such as packed towers, spray towers, venture scrubbers, bubble columns, and so forth. These mass-transfer contacting devices have several inevitable drawbacks such as difficulty of obtaining an accurate gas-liquid mass-transfer interfacial area, high capital and operating costs, limited range of gas and liquid flow rates due to operational problems such as flooding, foaming, and entrainment.

In recent years, a new technology has been extremely investigated, and processes using membrane-based contacting devices are promising. In these processes, membrane gas absorption technology and chemical absorption technology act together with advantages of both membrane reactor and gas-liquid absorption processes. Different membrane reactor geometries can be used for gas-liquid contacting but among these geometries hollow fiber membrane reactors (HFMRs) because of high surface-volume ratio found to be more efficient solution.[1] HFMRs compared to conventional gas absorption contacting devices aforementioned provide several practical advantages such as high specific surface area per unit reactor volume, independent control of gas and liquid flow rates without any flooding, loading, weeping, or foaming, known gas-liquid interfacial area, modularity, capable linear scale up or down, low corrosion problems, low capital, and operating costs.

Esato and Eiseman[2] were the first that used microporous membranes as gas-liquid reactors. They used flat membranes of polytetrafluoroethylene (PTFE) for the oxygenation of blood. Removal of the acid gases from flue gas streams by membrane reactors has been a research focus since 1980 and for this purpose; investigators have considered several factors such as absorption solutions, membrane specifications, and membrane modules to improve performance of acid gas removal. Qi and Cussler[3,4] were the first to develop the idea

Additional Supporting Information may be found in the online version of this article.

Correspondence concerning this article should be addressed to A. Molaei Dehkordi at amolaeid@sharif.edu

of the HFMR for CO_2 absorption using a microporous nonwetted polypropylene membrane and by means of aqueous sodium hydroxide solution. Feron and Jensen[5] used porous polyolefin membranes with novel solvents (CORAL) to remove CO_2 from various gas streams. Ren et al.[6] prepared polyvinylidene fluoride (PVDF) hollow fiber membranes for CO_2 capturing. The hollow fiber membranes were spun with two different dope solutions at various shear rates to examine the influences of the rheological characteristics of the dope solution on the membrane structure and the system performance for CO_2 absorption. Kreulen et al.[7] studied selective removal of H_2S from gas streams containing CO_2 and N_2. They used Methyldiethanolamine (MDEA) as the solvent and polypropylene and nylon 66 flat sheet membranes as nonwetted and wetted membranes, respectively. They found that nonwetted membranes decrease H_2S selectivity. Wang et al.[8] continued their research using tailor-made polyvinylidene fluoride hollow fiber membrane and sodium carbonate solution. They found that gas-to-liquid flow ratio and the CO_2 concentration have significant influence on the removal efficiency and H_2S selectivity. Boucif et al.[9] investigated hydrogen sulfide odor control; where in this study hydrogen sulfide odor control by absorption in water tanks to a hollow fiber reactor has been studied both experimentally and theoretically. Boucif et al.[10] conducted a mathematical and numerical investigation on the gas–liquid absorption of carbon dioxide by means of Monoethanolamine solution in an HFMR using microporous and nonporous membranes at identical operating parameters and reported higher performance for microporous membrane modules.

However, there are a few works dealing with mathematical modeling of multicomponent gas absorption particularly simultaneous absorption of CO_2 and H_2S. Coker and Freeman[11] performed one of the first multicomponent gas separation modeling using HFMRs. They concluded that for air separation, permeate purging with a small fraction of the residue stream provides a very effective method for improving module efficiency for drying but is not efficient for improving nitrogen purity or recovery. Faiz and Al-Marzouqi[12] performed a modeling study for the simultaneous absorption of CO_2 and H_2S with MEA as the solvent and verified their model predictions against experimental data for a special case in which pure water has been used as the solvent. Moreover, they found that low concentration of MEA can be efficient for the complete removal of H_2S, but increasing MEA concentration enhances CO_2 removal efficiency. Keshavarz et al.[13] performed their modeling study using Diethanolamine (DEA) as the absorbent and investigated the influences of wetting and operating parameters. They found that wetting has a great influence on CO_2 removal compared to H_2S; also, decreasing DEA concentration significantly decreases CO_2 removal.

In this work, a comprehensive mathematical model has been developed to investigate the dynamic behavior of HFMRs for the simultaneous chemical absorption of CO_2 and H_2S by means of MEA aqueous solution. The first goal of the present work was to develop a comprehensive model to obtain model predictions that have excellent agreement with experimental data reported in the literature. In this regard, to achieve this important goal, the previous model presented by Faiz and Al-Marzouqi[12] was significantly modified by

- Including thermal energy equation.
- Using equations of motion as a replacement of the assumption of fully developed velocity profiles.
- Dynamic modeling of the process.
- Analyzing the dynamic responses of HFMR to different step changes as the load.
- Evaluating the physical solubility of carbon dioxide and hydrogen sulfide as a function of the solvent temperature, solvent composition, and the gas pressure as a replacement of assumption of constant physical solubility.
- Taking into account the compressibility of the gas-phase mixture as a function of the gas temperature, gas pressure, and also the gas-phase composition.
- Taking into account the contribution of all molecular and convective terms in the governing equations such as the momentum equations, species continuity equations, and the thermal energy equations.

As the second goal of this work, the dynamic behavior and open-loop response of the reactor were analyzed carefully that can be useful for the process control purposes.

Mathematical Model

A schematic diagram of the reactor is shown in Figure 1. As it is shown in this figure, the solvent phase is introduced to the membrane reactor at $z=0$ in the tube side and the gas-phase mixture flows countercurrently and introduced at $z=L$ in the shell side. The present modeling approach is organized in four steps involving momentum, thermal energy, and mass transports such that all of them have been included. These are "Liquid in Tube," "Liquid in Membrane," "Gas in Membrane," and "Gas in Shell." These four parts are termed LT, LM, GM, and GS, respectively. The assumptions made in this work were as follows:

- Incompressible and Newtonian fluid flow for solvent flow.
- Total density and the concentration of gas-phase mixture were set to be a function of pressure, temperature, and the composition of the gas-phase mixture and estimated using an appropriate equation of state (EOS).
- The membrane and fluid flowing in it are at the thermal equilibrium. Therefore, the thermal energy equations for LM and GM were developed for the membrane and fluid together.
- Total concentration of the solvent phase was supposed to be constant.

Moreover, the dynamic behavior of the membrane reactor is analyzed carefully. In this regard, it was assumed that the gas and the solvent phases are stagnant at $t=0$, the reactor temperature is at T_{ic}, and there are no CO_2 and H_2S in the

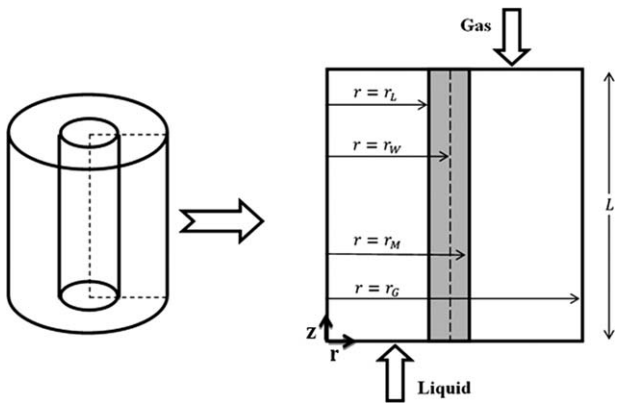

Figure 1. Schematic diagram of the reactor studied.

reaction system. At $t=0$, constant flow rates of the solvent and gas phases are suddenly introduced to the membrane reactor inlets. Thus, the governing equations can be expressed as

Momentum transport

LT.

$$\text{Continuity}: \frac{\partial V_{L_z}}{\partial z}+\frac{1}{r}\frac{\partial}{\partial r}(rV_{L_r})=0 \tag{1}$$

$$r-\text{Component}: \frac{\partial V_{L_r}}{\partial t}+V_{L_r}\frac{\partial V_{L_r}}{\partial r}+V_{L_z}\frac{\partial V_{L_r}}{\partial z} =-\frac{1}{\rho_L}\frac{\partial P_L}{\partial r}+\nu_{LT}\left(\frac{\partial}{\partial r}\left(\frac{1}{r}\frac{\partial}{\partial r}(rV_{L_r})\right)+\frac{\partial^2 V_{L_r}}{\partial z^2}\right) \tag{2}$$

$$\text{z}-\text{Component}: \frac{\partial V_{L_z}}{\partial t}+V_{L_r}\frac{\partial V_{L_z}}{\partial r}+V_{L_z}\frac{\partial V_{L_z}}{\partial z} =-\frac{1}{\rho_L}\frac{\partial P_L}{\partial z}+\nu_{LT}\left(\frac{1}{r}\frac{\partial}{\partial r}\left(r\frac{\partial V_{L_z}}{\partial r}\right)+\frac{\partial^2 V_{L_z}}{\partial z^2}\right) \tag{3}$$

The initial and boundary conditions imposed on the hydrodynamics for LT are as follows

$$\text{at } t=0, \text{for all } r \text{ and } z, \quad V_{L_z}=0, V_{L_r}=0 \tag{4}$$

$$\text{at } z=0, \text{for all } r, \quad V_{L_z}=U_{L_0}, V_{L_r}=0 \tag{5}$$

$$\text{at } z=L, \text{for all } r, \quad \frac{\partial V_{L_z}}{\partial z}=0, V_{L_r}=0 \tag{6}$$

$$\text{at } r=0, \text{for all } z, \quad \frac{\partial V_{L_z}}{\partial r}=0, V_{L_r}=0 \tag{7}$$

$$\text{at } r=r_L, \text{for all } z, \quad V_{L_z}=0, V_{L_r}=0 \tag{8}$$

LM and GM. Because of weak permeability of membranes used in the HFMRs, there is no significant bulk movement in the membrane thickness; hence, it was supposed that the fluid flow in the membrane is stagnant. The pore size in a porous medium has a profound influence on the Darcy flow and the mean pore size in typical membranes used in the hollow fiber membrane contactors can be taken as 0.167-μm (PVDF hollow fiber membrane contactor).[14] Note that the permeability of typical membranes used in these types of reactors is in an order of 10^{-15} m^2; hence, it could be assumed that these media are impermeable. It is well-known that the permeability can be evaluated by[15]

$$K=\frac{\varepsilon^3 d_p^2}{a(1-\varepsilon)} \tag{9}$$

where ε, d_p, and a are porosity, pore size, and a constant to parameterize the microscopic geometry of the porous medium, respectively.

GS. Using circular approximation[12] for the shell side geometry, Navier–Stokes equations for the gas-phase mixture flow in the shell side accounting for all molecular and convective terms can be expressed as

$$\text{Continuity}: \frac{\partial(\rho_G)}{\partial t}+\frac{1}{r}\frac{\partial}{\partial r}(r\rho_G V_{G_r})+\frac{\partial}{\partial z}(\rho_G V_{G_z})=0 \tag{10}$$

$$r\text{-Component}: \frac{\partial(\rho_G V_{G_r})}{\partial t}+\frac{1}{r}\frac{\partial}{\partial r}(r\rho_G V_{G_r}V_{G_r}) +\frac{\partial}{\partial z}(\rho_G V_{G_z}V_{G_r})=-\frac{\partial P_G}{\partial r}-\left(\frac{1}{r}\frac{\partial}{\partial r}(r\tau_{rr})+\frac{\partial}{\partial z}(\tau_{zr})+\frac{\tau_{\theta\theta}}{r}\right) \tag{11}$$

$$z-\text{Component}: \frac{\partial(\rho_G V_{G_z})}{\partial t}+\frac{1}{r}\frac{\partial}{\partial r}(r\rho_G V_{G_r}V_{G_z}) +\frac{\partial}{\partial z}(\rho_G V_{G_z}V_{G_z})=-\frac{\partial P_G}{\partial z}-\left(\frac{1}{r}\frac{\partial}{\partial r}(r\tau_{rz})+\frac{\partial}{\partial z}(\tau_{zz})\right) \tag{12}$$

where

$$\tau_{rr}=\frac{2}{3}\mu_G(\nabla.V_G)-2\mu_G\frac{\partial V_{G_r}}{\partial r}$$

$$\tau_{zz}=\frac{2}{3}\mu_G(\nabla.V_G)-2\mu_G\frac{\partial V_{G_z}}{\partial z}$$

$$\tau_{\theta\theta}=\frac{2}{3}\mu_G(\nabla.V_G)-2\mu_G\frac{V_{G_r}}{r} \tag{13}$$

$$\tau_{zr}=\tau_{rz}=-\mu_G\left(\frac{\partial V_{G_z}}{\partial r}+\frac{\partial V_{G_r}}{\partial z}\right)$$

Moreover, the initial and boundary conditions for the momentum equations for the gas-phase mixture are as follows

$$\text{at } t=0, \text{for all } r \text{ and } z, \quad V_{G_z}=0, V_{G_r}=0 \tag{14}$$

$$\text{at } z=0, \text{for all } r, \quad \frac{\partial V_{G_z}}{\partial z}=0, V_{G_r}=0 \tag{15}$$

$$\text{at } z=L, \text{for all } r, \quad V_{G_z}=-U_{G_0}, V_{G_r}=0 \tag{16}$$

$$\text{at } r=r_M, \text{for all } z, \quad V_{G_z}=0, V_{G_r}=0 \tag{17}$$

$$\text{at } r=r_G, \text{for all } z, \quad \frac{\partial V_{G_z}}{\partial r}=0, V_{G_r}=0 \tag{18}$$

Thermal energy balance

LT. The thermal energy equation for the solvent flowing in the tube side and taking into account the viscous dissipation due to viscous heating and enthalpy change of reactions can be simplified to

$$\frac{\partial T_{\text{LT}}}{\partial t}+V_{L_r}\frac{\partial T_{\text{LT}}}{\partial r}+V_{L_z}\frac{\partial T_{\text{LT}}}{\partial z}=\alpha_{\text{LT}}\left(\frac{1}{r}\frac{\partial}{\partial r}\left(r\frac{\partial T_{\text{LT}}}{\partial r}\right)+\frac{\partial^2 T_{\text{LT}}}{\partial z^2}\right) +\frac{\mu_{\text{LT}}}{\rho_{\text{LT}}C_{p_{\text{LT}}}}\Phi_{\nu_{LT}}+\frac{\sum_i(R_i\Delta H_{R_i})}{\rho_{\text{LT}}C_{p_{\text{LT}}}} \tag{19}$$

where $\Phi_{\nu_{\text{LT}}}$ is the viscous dissipation term that can be expressed as

$$\Phi_{\nu_{\text{LT}}}=2\left(\left(\frac{\partial V_{L_r}}{\partial r}\right)^2+\left(\frac{\partial V_{L_z}}{\partial z}\right)^2+\left(\frac{V_{L_r}}{r}\right)^2\right)+\left(\frac{\partial V_{L_r}}{\partial z}+\frac{\partial V_{L_z}}{\partial r}\right)^2 \tag{20}$$

The last term in Eq. 19 refers to the heat generation due to the chemical reactions that occur in the solvent phase. The initial and boundary conditions imposed on the thermal energy equation for the LT case are as follows

$$\text{at } t=0, \text{for all } r \text{ and } z, \quad T_{\text{LT}}=T_{\text{ic}} \tag{21}$$

$$\text{at } z=0, \text{for all } r, \quad T_{\text{LT}}=T_{L_0} \tag{22}$$

$$\text{at } z=L, \text{for all } r, \quad \frac{\partial^2 T_{\text{LT}}}{\partial z^2}=0 \tag{23}$$

$$\text{at } r=0, \text{for all } z, \quad \frac{\partial T_{\text{LT}}}{\partial r}=0 \tag{24}$$

$$\text{at } r=r_L, \text{for all } z, \qquad -k_{\mathrm{LT}}\frac{\partial T_{\mathrm{LT}}}{\partial r}=-k_{\mathrm{LM}}\frac{\partial T_{\mathrm{LM}}}{\partial r}, T_{\mathrm{LT}}=T_{\mathrm{LM}} \tag{25}$$

LM. In the absence of the bulk movement in the membrane thickness, the convective terms in the thermal energy equation for the LM case and the membrane could be dropped. Moreover, there is no viscous dissipation in this region of reactor, therefore, we have

$$\frac{\partial T_{\mathrm{LM}}}{\partial t}=\alpha_{\mathrm{LM}}\left(\frac{1}{r}\frac{\partial}{\partial r}\left(r\frac{\partial T_{\mathrm{LM}}}{\partial r}\right)+\frac{\partial^2 T_{\mathrm{LM}}}{\partial z^2}\right)+\frac{\sum_i (R_i \Delta H_{R_i})}{\rho_{\mathrm{LM}} C_{p_{\mathrm{LM}}}} \tag{26}$$

Note that it was supposed that the membrane and the solvent flowing in it are at the thermal equilibrium. The initial and boundary conditions imposed on Eq. 26 are presented in Eqs. 27–31

$$\text{at } t=0, \text{for all } r \text{ and } z, \qquad T_{\mathrm{LM}}=T_{\mathrm{ic}} \tag{27}$$

$$\text{at } z=0, \text{for all } r, \qquad \frac{\partial T_{\mathrm{LM}}}{\partial z}=0 \tag{28}$$

$$\text{at } z=L, \text{for all } r, \qquad \frac{\partial T_{\mathrm{LM}}}{\partial z}=0 \tag{29}$$

$$\text{at } r=r_L, \text{for all } z, \qquad -k_{\mathrm{LM}}\frac{\partial T_{\mathrm{LM}}}{\partial r}=-k_{\mathrm{LT}}\frac{\partial T_{\mathrm{LT}}}{\partial r}, T_{\mathrm{LM}}=T_{\mathrm{LT}} \tag{30}$$

$$\text{at } r=r_W, \text{for all } z, \quad -k_{\mathrm{LM}}\frac{\partial T_{\mathrm{LM}}}{\partial r}=-k_{\mathrm{GM}}\frac{\partial T_{\mathrm{GM}}}{\partial r}-\sum_{\mathrm{i}} N_i \Delta H_{s_i}, T_{\mathrm{LM}}=T_{\mathrm{GM}} \tag{31}$$

The enthalpy change of solutions and the reactions for these systems are in the same order of magnitude. Therefore, as it is seen in Eq. 31, the enthalpy changes of solution for diffusing components (i.e., CO_2 and H_2S) were also taken into account.

GM. Chemical reactions occur only in the solvent phase, and there is no chemical reaction in the gas-phase mixture. Considering this fact, the thermal energy equation for the gas and membrane that are at the thermal equilibrium, is simplified to

$$\frac{\partial \rho_{\mathrm{GM}} T_{\mathrm{GM}}}{\partial t}=\frac{k_{\mathrm{GM}}}{C_{p_{\mathrm{GM}}}}\left(\frac{1}{r}\frac{\partial}{\partial r}\left(r\frac{\partial T_{\mathrm{GM}}}{\partial r}\right)+\frac{\partial^2 T_{\mathrm{GM}}}{\partial z^2}\right) \tag{32}$$

subject to the following initial and boundary conditions

$$\text{at } t=0, \text{for all } r \text{ and } z, \qquad T_{\mathrm{GM}}=T_{\mathrm{ic}} \tag{33}$$

$$\text{at } z=0, \text{for all } r, \qquad \frac{\partial T_{\mathrm{GM}}}{\partial z}=0 \tag{34}$$

$$\text{at } z=L, \text{for all } r, \qquad \frac{\partial T_{\mathrm{GM}}}{\partial z}=0 \tag{35}$$

$$\text{at } r=r_W, \text{for all } z, \quad -k_{\mathrm{GM}}\frac{\partial T_{\mathrm{GM}}}{\partial r}=-k_{\mathrm{LM}}\frac{\partial T_{\mathrm{LM}}}{\partial r}+\Sigma N_i \Delta H_{s_i}, T_{\mathrm{GM}}=T_{\mathrm{LM}} \tag{36}$$

$$+\mathrm{Da}_{\mathrm{HS}^-{}_1}\ C^*_{\mathrm{H_2S_{LM}}} C^*_{\mathrm{MEA_{LM}}} - \mathrm{Da}_{\mathrm{HS}^-{}_2} C^*_{\mathrm{HS}^-{}_{\mathrm{LM}}} C^*_{\mathrm{MEAH}^+{}_{\mathrm{LM}}} \tag{37}$$

GS. The only difference between the thermal energy equations for GS and LT is the existence of chemical reactions and density variation that can be estimated by an EOS such as the Peng-Robinson EOS. As mentioned earlier, there is no chemical reaction in the gas-phase mixture; therefore, using circular approximation[12] for the shell side geometry, the thermal energy equation can be expressed as

$$\frac{\partial \rho_{\mathrm{GS}} T_{\mathrm{GS}}}{\partial t}+\frac{1}{r}\frac{\partial r \rho_{\mathrm{GS}} V_{G_r} T_{\mathrm{GS}}}{\partial r}+\frac{\partial \rho_G V_{G_z} T_{\mathrm{GS}}}{\partial z} =\frac{k_{\mathrm{GS}}}{C_{p_{\mathrm{GS}}}}\left(\frac{1}{r}\frac{\partial}{\partial r}\left(r\frac{\partial T_{\mathrm{GS}}}{\partial r}\right)+\frac{\partial^2 T_{\mathrm{GS}}}{\partial z^2}\right)+\frac{\mu_{\mathrm{GS}}}{C_{p_{\mathrm{GS}}}}\Phi_{v_{\mathrm{GS}}} \tag{38}$$

where $\Phi_{v_{\mathrm{GS}}}$ is the viscous dissipation term the same as Eq. 20, just by replacing V_{L_r} and V_{L_z} with V_{G_r} and V_{G_z}, respectively. Corresponding initial and boundary conditions are as follows

$$\text{at } t=0, \text{for all } r \text{ and } z, \qquad T_{\mathrm{GS}}=T_{\mathrm{ic}} \tag{39}$$

$$\text{at } z=0, \text{for all } r, \qquad \frac{\partial^2 T_{\mathrm{GS}}}{\partial z^2}=0 \tag{40}$$

$$\text{at } z=L, \text{for all } r, \qquad T_{\mathrm{GS}}=T_{G_0} \tag{41}$$

$$\text{at } r=r_M, \text{for all } z, \qquad -k_{\mathrm{GS}}\frac{\partial T_{\mathrm{GS}}}{\partial r}=-k_{\mathrm{GM}}\frac{\partial T_{\mathrm{GM}}}{\partial r}, T_{\mathrm{GS}}=T_{\mathrm{GM}} \tag{42}$$

$$\text{at } r=r_G, \text{for all } z, \qquad \frac{\partial T_{\mathrm{GS}}}{\partial r}=0 \tag{43}$$

Mass transport

Reaction scheme: The chemical reactions occurred in the solvent phase can be expressed as[12]

- Reaction kinetics for carbon dioxide with MEA[12,16]

Reaction mechanism can be separated in two steps; first, the formation of zwitterion and second the removal of a proton amine

$$CO_2+RNH_2 \overset{k_{r_{CO_2-MEA}},k_{-r_{CO_2-MEA}}}{\Longleftrightarrow} RNH_2^+COO^- \tag{44}$$

$$RNH_2^+COO^- + RNH_2 \overset{k_{r_{RNH_2^+COO^-}}}{\Rightarrow} RNHCOO^- + RNH_3^+ \tag{45}$$

The overall reaction rate for CO_2 decomposition can be expressed as

$$r_{CO_2}=\frac{k_{r_{CO_2-MEA}} C_{CO_{2_L}} C_{MEA_L}}{1+\frac{k_{-r_{CO_2-MEA}}}{k_{r_{RNH_2^+COO^-}} C_{MEA_L}}} \tag{46}$$

when $\frac{k_{-r_{CO_2-MEA}}}{k_{r_{RNH_2^+COO^-}} C_{MEA_L}} << 1$ (Assuming almost irreversible reaction between CO_2 and MEA), Eq. 46 can be simplified to

$$r_{CO_2}=-k_{r_{CO_2-MEA}}\ C_{CO_{2_L}} C_{MEA_L} \tag{47}$$

Besides, carbomate formation rate can be expressed as

$$r_{MEACOO^-}=+k_{r_{CO_2-MEA}}\ C_{CO_{2_L}} C_{MEA_L} \tag{48}$$

- Reaction kinetics for hydrogen sulfide with MEA[12]

First, hydrogen sulfide reacts with MEA to produce proton amine and hydrosulfide that involves only proton transfer from H_2S to MEA. It can be assumed that this reaction is instantaneous[17] and, therefore, one may consider H_2S-MEA equilibrium in the entire solvent phase at each time of the process.[12] Second, deprotonated hydrogen sulfide reacts with

MEA to produce proton amine and sulfide ion as expressed by

$$H_2S+MEA \overset{k_{r_{H_2S-MEA}}}{\Rightarrow} MEAH^+ + HS^- \tag{49}$$

$$HS^- + MEA \overset{K_{eq\,MEA-HS^-}}{\Rightarrow} MEAH^+ + S^{2-} \tag{50}$$

The overall reaction rates of the involving components may be expressed with the following expressions

$$r_{H_2S} = -k_{r_{H_2S-MEA}} \left(C_{H_2S_L} C_{MEA_L} - \frac{C_{HS^-{}_L} C_{MEAH^+{}_L}}{K_{eq\,MEA-HS^-}} \right) \tag{51}$$

$$r_{HS^-} = +k_{r_{H_2S-MEA}} \left(C_{H_2S_L} C_{MEA_L} - \frac{C_{HS^-{}_L} C_{MEAH^+{}_L}}{K_{eq\,MEA-HS^-}} \right) \tag{52}$$

Moreover, overall reaction rates for MEA and the proton amine can be expressed as

$$r_{MEA} = -2k_{r_{CO_2-MEA}} C_{CO_{2_L}} C_{MEA_L} - k_{r_{H_2S-MEA}} \left(C_{H_2S_L} C_{MEA_L} - \frac{C_{HS^-{}_L} C_{MEAH^+{}_L}}{K_{eq\,MEA-HS^-}} \right) \tag{53}$$

$$r_{MEAH^+} = k_{r_{CO_2-MEA}} \; C_{CO_{2_L}} C_{MEA_L} + k_{r_{H_2S-MEA}} \left(C_{H_2S_L} C_{MEA_L} - \frac{C_{HS^-{}_L} C_{MEAH^+{}_L}}{K_{eq\,MEA-HS^-}} \right) \tag{54}$$

LT. The species continuity equation for the solvent phase flowing in the tube can be simplified to

$$\frac{\partial C_{i_{LT}}}{\partial t} + \frac{1}{r}\frac{\partial}{\partial r}(rV_{L_r} C_{i_{LT}}) + \frac{\partial}{\partial z}(V_{L_z} C_{i_{LT}}) = D_{i_{LT}} \left(\frac{1}{r}\frac{\partial}{\partial r}\left(r\frac{\partial C_{i_{LT}}}{\partial r} \right) + \frac{\partial^2 C_{i_{LT}}}{\partial z^2} \right) + R_i \tag{55}$$

where subscript i stands for carbon dioxide, hydrogen sulfide, hydrosulfide, carbomate, proton amine, and MEA. The initial and boundary conditions for these equations are as follows

$$\text{at } t=0, \text{for all } r \text{ and } z, \qquad C_{i_{LT}} = C_{i_{L_0}} \tag{56}$$

$$\text{at } z=0, \text{for all } r, \qquad C_{i_{LT}} = C_{i_{L_0}} \tag{57}$$

$$\text{at } z=L, \text{for all } r, \qquad \frac{\partial^2 C_{i_{LT}}}{\partial z^2} = 0 \tag{58}$$

$$\text{at } r=0, \text{for all } z, \qquad \frac{\partial C_{i_{LT}}}{\partial r} = 0 \tag{59}$$

$$\text{at } r=r_L, \text{for all } z, \qquad -D_{i_{LT}} \frac{\partial C_{i_{LT}}}{\partial r} = -D_{i_{LM}} \frac{\partial C_{i_{LM}}}{\partial r}, \; C_{i_{LT}} = C_{i_{LM}} \tag{60}$$

LM. In this case, there is no velocity and bulk movement; therefore, the governing equations for mass transfers are simplified to

$$\frac{\partial C_{i_{LM}}}{\partial t} = D_{i_{LM}} \left(\frac{1}{r}\frac{\partial}{\partial r}\left(r\frac{\partial C_{i_{LM}}}{\partial r} \right) + \frac{\partial^2 C_{i_{LM}}}{\partial z^2} \right) + R_i \tag{61}$$

subject to the following initial and boundary conditions

$$\text{at } t=0, \text{for all } r \text{ and } z, \qquad C_{i_{LM}} = C_{i_{L_0}} \tag{62}$$

$$\text{at } z=0, \text{for all } r, \qquad \frac{\partial C_{i_{LM}}}{\partial z} = 0 \tag{63}$$

$$\text{at } z=L, \text{for all } r, \qquad \frac{\partial C_{i_{LM}}}{\partial z} = 0 \tag{64}$$

$$\text{at } r=r_L, \text{for all } z, \quad -D_{i_{LM}} \frac{\partial C_{i_{LM}}}{\partial r} = -D_{i_{LT}} \frac{\partial C_{i_{LT}}}{\partial r}, \; C_{i_{LM}} = C_{i_{LT}} \tag{65}$$

At the interface of the solvent and gas phases, the important point is that only carbon dioxide and hydrogen sulfide can transfer between two phases and it was supposed that MEA, $MEACOO^-$, $MEAH^+$, and HS^- could not transfer to the gas phase. Therefore, for the nondiffusing components (i.e., MEA, $MEACOO^-$, $MEAH^+$, and HS^-), the concentration gradient at the interface was set to zero, whereas for diffusing components (i.e., CO_2 and H_2S), the boundary conditions can be expressed as

$$\text{at } r=r_W, \text{for all } z, \quad -D_{i_{LM}} \frac{\partial C_{i_{LM}}}{\partial r} = -D_{i_{GM}} C_{tot_{GM}} \frac{\partial y_{i_{GM}}}{\partial r}, \quad C_{i_{LM}} = \frac{y_{i_{GM}}}{m_i} \tag{66}$$

where the modified Henry's constant (i.e., m_i) can be evaluated by

$$m_i = \frac{1}{C_{tot_L} P_G} H_i \tag{67}$$

As it is obvious from Eq. 67, the modified Henry's constant was set to be a function of gas pressure, interface temperature, and composition of the solvent phase at the interface of gas and solvent phases in which the solvent temperature and composition are included in H_i. Although it was supposed that the concentration of the solvent phase is constant throughout the reactor, Henry's constant of a species which is at equilibrium with the mixture of liquids could be related to its Henry's constants corresponding to the pure liquids by the following equation[18]

$$\ln(H_{i_{mix}}) = \Sigma\left(x_j \ln\left(H_{i_j} \right) \right) \tag{68}$$

GM. The governing equations are just the same as LM case except that there is no reaction in the gas phase. Moreover, the total density of the gas phase is a function of pressure, temperature, and composition that can be evaluated by an EOS (i.e., Peng–Robinson equation of state).[19] Thus, the governing equations are presented below without any additional explanations

$$\frac{\partial C_{tot_{GM}} y_{i_{GM}}}{\partial t} = D_{i_{GM}} \left(\frac{1}{r}\frac{\partial}{\partial r}\left(rC_{tot_{GM}} \frac{\partial y_{i_{GM}}}{\partial r} \right) + \frac{\partial}{\partial z}\left(C_{tot_{GM}} \frac{\partial y_{i_{GM}}}{\partial z} \right) \right) \tag{69}$$

subject to the following initial and boundary conditions

$$\text{at } t=0, \text{for all } r \text{ and } z, \qquad y_{i_{GM}} = 0 \tag{70}$$

$$\text{at } z=0, \text{for all } r, \qquad \frac{\partial y_{i_{GM}}}{\partial z} = 0 \tag{71}$$

$$\text{at } z=L, \text{for all } r, \qquad \frac{\partial y_{i_{GM}}}{\partial z} = 0 \tag{72}$$

$$\text{at } r=r_W, \text{for all } z, \quad -D_{i_{GM}} C_{tot_{GM}} \frac{\partial y_{i_{GM}}}{\partial r} = -D_{i_{LM}} \frac{\partial C_{i_{LM}}}{\partial r}, \; y_{i_{GM}} = mC_{i_{LM}} \tag{73}$$

$$\text{at } r=r_M, \text{for all } z, \qquad -D_{i_{GM}} \frac{\partial y_{i_{GM}}}{\partial r} = -D_{i_{GS}} \frac{\partial y_{i_{GS}}}{\partial r}, \; y_{i_{GM}} = y_{i_{GS}} \tag{74}$$

Table 1. Specification of the Hollow Fiber Membrane Reactor[20]

Parameter	Value
Inner tube diameter (mm)	0.344
Outer tube diameter (mm)	0.442
Gas shell diameter (mm)	0.780
Module length (cm)	80
Number of fibers	7000
ε (porosity)	0.45
τ (tortuosity)	2

GS. Using circular and axisymmetric approximation[12] for the shell side geometry, the species continuity equations for the gas-phase mixture are simplified to

$$\frac{\partial C_{\text{tot}_{GS}} y_{i_{GS}}}{\partial t} + \frac{1}{r}\frac{\partial}{\partial r}\left(rV_{G_r} C_{\text{tot}_{GS}} y_{i_{GS}}\right) + \frac{\partial}{\partial z}\left(V_{G_z} C_{\text{tot}_{GS}} y_{i_{GS}}\right) = D_{i_{GS}}\left(\frac{1}{r}\frac{\partial}{\partial r}\left(rC_{\text{tot}_{GS}}\frac{\partial y_{i_{GS}}}{\partial r}\right) + \frac{\partial}{\partial z}\left(C_{\text{tot}_{GS}}\frac{\partial y_{i_{GS}}}{\partial z}\right)\right) \tag{75}$$

subject to the following initial and boundary conditions

$$\text{at } t=0, \text{for all } r \text{ and } z, \qquad y_{i_{GS}} = 0 \tag{76}$$

$$\text{at } z=0, \text{for all } r, \qquad \frac{\partial^2 y_{i_{GS}}}{\partial z^2} = 0 \tag{77}$$

$$\text{at } z=L, \text{for all } r, \qquad y_{i_{GS}} = y_{i_{G_0}} \tag{78}$$

$$\text{at } r=r_M, \text{for all } z, \qquad -D_{i_{GS}}\frac{\partial y_{i_{GS}}}{\partial r} = -D_{i_{GM}}\frac{\partial y_{i_{GM}}}{\partial r}, \; y_{i_{GS}} = y_{i_{GM}} \tag{79}$$

$$\text{at } r=r_G, \text{for all } z, \qquad \frac{\partial y_{i_{GS}}}{\partial r} = 0 \tag{80}$$

Input Data

In this work, some physical and chemical properties are strong function of pressure, temperature, and composition of each phase; hence, it was decided to take into account all these effects. But for some cases, we are unable to found an appropriate functionality.

Specifications of the HFMR studied in this work are presented in Table 1. In addition, physical and chemical properties of the solvent and the gas-phase mixture are given in Tables 2 and 3, respectively. Note that molecular diffusivities of $MEAH^+$ and $MEACOO^-$ were supposed to be equal to that of MEA and similarly the molecular diffusivity of HS^- was taken equal to the molecular diffusivity of H_2S.[12] Moreover, molecular diffusivity of each species in the fluid within the membrane can be evaluated by[13]

$$D_{i-\text{membrane}} = \frac{D_i \times \varepsilon}{\tau} \tag{81}$$

where, D_i, $D_{i-\text{membrane}}$, ε, and τ are actual and apparent molecular diffusivity of the component i, membrane porosity, and membrane tortuosity, respectively.

As it is shown in Table 2, because of almost instantaneous reaction between hydrogen sulfide and MEA, the rate constant of this reaction was set to be temperature independent. The Henry's constants of carbon dioxide in pure MEA and pure water are presented in Table 4. Moreover, due to lack of equilibrium data for H_2S-MEA-Water, we put the Henry's constants of H_2S in pure MEA and pure water equal to 60 and 54 MPa, respectively.[13] Then, using Eq. 68, Henry's constant for each species (i.e., CO_2 and H_2S) in the MEA aqueous solution could be evaluated.

Numerical Analysis

The dimensionless forms of the governing equations derived in the developed mathematical model are presented in Supporting Information, Appendix A. These dimensionless governing equations were solved numerically subject to the corresponding dimensionless initial and boundary conditions. Reactions occurred in the solvent phase cause to have relatively stiff set of equations; in addition, large reaction rate constant of H_2S decomposition compared to that of CO_2 leads to wide range order of magnitude of eigenvalues. Therefore, we had to choose fine mesh sizes in the solvent phase to predict the concentration gradient in this region precisely. Thus, explicit method needs a very small time step and this is not an appropriate numerical scheme. The

Table 2. Physical and Chemical Properties of the Liquid Phase (i.e., Solvent)

Parameter	Value	References
μ_{H_2O} (Pa .s)	10^{-3}	Ashrae[21]
μ_{MEA} (Pa .s)	1.5×10^{-2}	Akanksha et al.[22]
ρ_{H_2O} (kg/m^3)	1000	Ashrae[21]
ρ_{MEA} (kg/m^3)	1012	Akanksha et al.[22]
$C_{p_{H_2O}}$ (kJ/kg .K)	4.18	Ashrae[21]
$C_{p_{MEA}}$ (kJ/kg .K)	2.8424	Akanksha et al.[22]
k_{H_2O} (kW/m .K)	6×10^{-4}	Ashrae[21]
k_{MEA} (kW/m .K)	2.96×10^{-4}	Akanksha et al.[22]
D_{CO_2} (m^2/s)	1.51×10^{-9}	Faiz and Al-Marzouqi[12]
D_{H_2S} (m^2/s)	1.52×10^{-9}	Faiz and Al-Marzouqi[12]
D_{MEA} (m^2/s)	9.32×10^{-10}	Faiz and Al-Marzouqi[12]
$k_{r_{CO_2\text{-}MEA}}$ (m^3/mol .s)	$10^{(10.99-2152/T)}/1000$	Faiz and Al-Marzouqi[12]
$K_{eq_{MEA-HS^-}}$	295	Faiz and Al-Marzouqi[12]
$k_{r_{H_2S\text{-}MEA}}$ (m^3/mol .s)	10^6	Faiz and Al-Marzouqi[12]
$\Delta H_{R_{CO_2}}$ (kJ/mol)	−83.921	Polasek and Bullin[23]
$\Delta H_{R_{H_2S}}$ (kJ/mol)	−43.841	Polasek and Bullin[23]
$\Delta H_{s_{CO_2}}$ (kJ/mol)	−19.4	Akanksha et al.[22]
$\Delta H_{s_{H_2S}}$ (kJ/mol)	−13.8	Burgess and Germann[24]

Table 3. Physical and Chemical Properties of the Gas Phase

Parameter	Value	References
μ_{CH_4} (Pa .s)	1.15×10^{-5}	Ashrae[21]
$C_{p_{CH_4}}$ (kJ/kg .K)	2.18	Ashrae[21]
k_{CH_4} (kW/m .K)	3.281×10^{-5}	Ashrae[21]
D_{CO_2} (m^2/s)	1.8×10^{-5}	Faiz and Al-Marzouqi[12]
D_{H_2S} (m^2/s)	2.01×10^{-5}	Faiz and Al-Marzouqi[12]

solution method used in this work was based on the ADI method using second-order error of central difference approximation for radial and axial molecular terms and first-order upwind method for the convective terms.[26] Using ADI method after Newton linearization, the set of governing equations could be transformed into a set of linear equations, which could be solved by linear algebra algorithms. The sensitivity of the present numerical solution to the mesh number or mesh size was examined carefully. This was performed to choose an appropriate grid size for the entire computation domains. The radial grid sizes chosen in this work are not equal for the entire domain and due to reactive conditions of LM, smaller step sizes were applied for this region. It was found that for step sizes smaller than $\Delta z^* = 0.01$, $\Delta r^*_{LT} = 0.05$, $\Delta r^*_{LM} = 0.005$, $\Delta r^*_{GM} = 0.01$, and $\Delta r^*_{GS} = 0.01$, there is no sensitivity to the grid sizes and the model predictions did not vary significantly. Thus, these values were chosen as the appropriate grid sizes for the present numerical computation. Therefore, all simulation results were obtained by the aforementioned grid sizes.

Results and Discussion

The obtained results and related discussions of the present work are presented in three subsections that are steady-state behavior, dynamic behavior, and analysis of open-loop response of the reactor. It should be noted that all of the presented simulation data were obtained using the Peng–Robinson equation of state for the prediction of gas-phase density as a function of the gas-phase temperature, pressure, and composition.

Steady-state analysis

Predictions of the steady-state behavior of simultaneous absorption of CO_2 and H_2S using MEA aqueous solution in HFMRs have been studied in previous works; but in this part of the present work, it was tried to present a comprehensive model for the improvement of predictions and achieving excellent agreement with the experimental data. In the following, it is shown that the complications can be so important and should be included in the developed model.

To analyze the hydrodynamics of the reactor, Figures 2a, b are presented for the solvent and gas phases, respectively. These figures demonstrate a good trend of achieving fully developed conditions. As it may be observed from Figures 2a, b, as the flow patterns tend to fully developed regimes, average radial velocities of streams diminish. The average radial velocity of gas and solvent phases can be evaluated by the following relations

$$V_{L_{r_{Ave}}} = \frac{\int_0^{r_L} V_{L_r} 2\pi r dr}{\int_0^{r_L} 2\pi r dr} \tag{82}$$

$$V_{G_{r_{Ave}}} = \frac{\int_{r_M}^{r_G} V_{G_r} 2\pi r dr}{\int_{r_M}^{r_G} 2\pi r dr} \tag{83}$$

Although exothermic reactions occur in the solvent phase, low concentration levels of CO_2 and H_2S in the solvent phase lead to low reaction rates and also, because of relatively small value of heat of reactions, there is no major axial temperature gradient in the solvent phase (about $\Delta T \cong 3^\circ C$ in the axial coordinate for the case study). Nevertheless, significant temperature gradient is observed in the gas phase. Figure 3 shows the average temperature variations for both the phases at different inlet solvent and gas temperatures. The average temperatures of the gas and solvent phases can be evaluated by

$$T_{L_{Ave}} = \frac{\int_0^{r_L} V_{L_z} \rho_L C_{p_L} T_L 2\pi r dr}{\int_0^{r_L} V_{L_z} \rho_L C_{p_L} 2\pi r dr} \tag{84}$$

$$T_{G_{Ave}} = \frac{\int_{r_M}^{r_G} V_{G_z} \rho_G C_{p_G} T_G 2\pi r dr}{\int_{r_M}^{r_G} V_{G_z} \rho_G C_{p_G} 2\pi r dr} \tag{85}$$

The gas-phase temperature varies and tends to the inlet solvent temperature that can be explained by this fact that the Peclet number value for the liquid phase is larger than that for the gas-phase mixture. Thus, the reason of accounting the thermal energy equation in the present model can be justified by this fact that although, the solvent-phase temperature is not varied significantly through the reactor, for accurate predictions of the gas-phase temperature, the thermal energy equation should be included.

To show the superiority of the developed model for the prediction of the effects of the gas pressure on the reactor performance and also evaluating the reactor behavior even at high pressures, the simulation results of the present model for different inlet gas pressures were compared against available experimental data reported by Marzouk et al.[27] Figure 4 demonstrates the present model predictions and experimental data for CO_2 and H_2S fluxes[12] as a function of pressures up to 5000 kPa. As can be observed from this figure, the developed model can predict the reactor behavior accurately. It should be noted that models with incompressible fluid flow assumption for the gas phase would probably fail to predict accurate results for the experimental data under such high-pressure conditions. This expectable failure can be explained

Table 4. Henry's Constants of CO_2 in MEA and Water[25] ($Ln\ H_{i-j}(\text{Pa}) = C_1 + \frac{C_2}{T} + C_3 Ln\ T + C_4 T$)

$i-j$	C_1	C_2	C_3	C_4
CO_2-H_2O	170.7126	−8477.711	−21.95743	0.005780748
CO_2−MEA	89.452	−2934.6	−11.592	0.01644

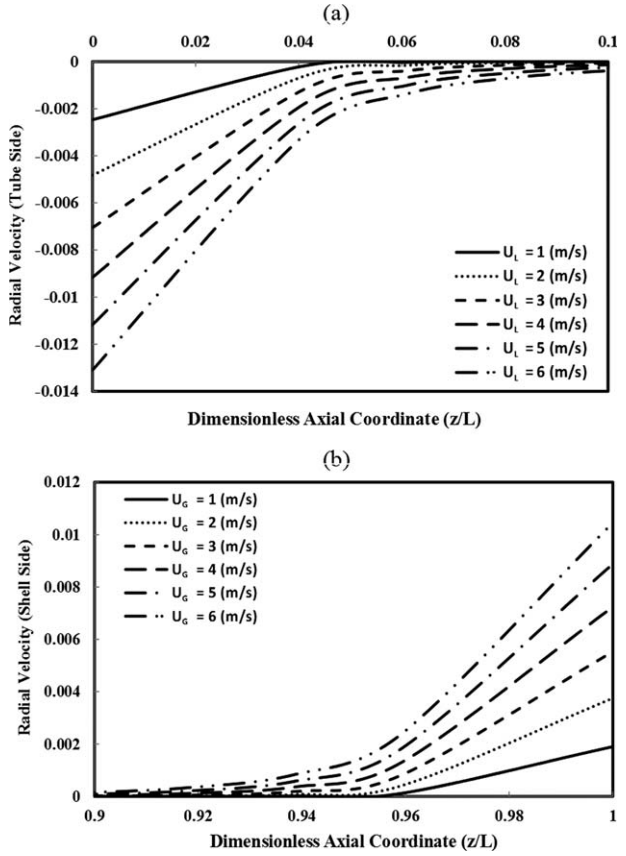

Figure 2. Variations of dimensionless average radial velocity with the reactor's length.

(a) Liquid in the tube side (i.e., LT), inlet liquid temperature = 308 K, MEA concentration = 1.0 M, (b) gas in the shell side (i.e., GS), inlet gas temperature = 298 K, inlet gas pressure = 100 kPa, gas feed: 0.15 CO_2 and 0.05 H_2S.

by this fact that with the assumption of incompressible gas flow, the effect of increasing the gas pressure would be the same as increasing the concentration of diffusing components (i.e., CO_2 and H_2S). To make this issue more clear, note that in simplified models, the only significant role of the pressure value is in the determination of the inlet gas concentration or density and, therefore, increasing the gas-phase pressure would result in increasing the gas-phase concentration. However, the present model can take into account both the compressibility of the gas phase and the entrance region of momentum transfer as two important issues that the total pressure of the gas phase can affect them; hence, it is possible to have excellent predictions at such conditions. The necessity of the two mentioned important factors that the simplified models cannot consider, are as follows: (1) by increasing the total pressure of the inlet gas, pressure gradient would be increased that this effect is not considered in the simplified model because of lack of accounting the entrance region of momentum transfer and assuming constant pressure for the whole process; and (2) considering the variations of the pressure in the gas side of the reactor, there would be a significant attention in the variations of the gas density, especially at high pressures, whereas the simplified models cannot consider this important effect.

Both the reactor performance and the concentration gradient in the gas phase are the most important parameters, which should be studied. To present the obtained simulation results, the average concentration of carbon dioxide in the gas-phase mixture was evaluated by the following expression

$$C_{G_{\text{Ave}}} = \frac{\int_{r_M}^{r_G} V_{G_z} C_{\text{tot}_G} y_G 2\pi r dr}{\int_{r_M}^{r_G} V_{G_z} 2\pi r dr} \tag{86}$$

In addition, the reactor performance can be expressed as

$$\text{Performance} = \frac{(QC_i)_{\text{inlet}} - (QC_i)_{\text{outlet}}}{(QC_i)_{\text{inlet}}} \tag{87}$$

where Q and C_i are volumetric gas flow rate and concentration of the diffusing components (i.e., CO_2 and H_2S), respectively.

With an increase in the inlet gas velocity, both carbon dioxide and hydrogen sulfide removals decrease. For large velocities of the gas-phase mixture, there is no enough residence time for removing the diffusing components from the gas-phase mixture. Figure 5 shows the effect of inlet gas velocity on the reactor performance and as it is expected, the performance of the reactor increases for smaller inlet gas

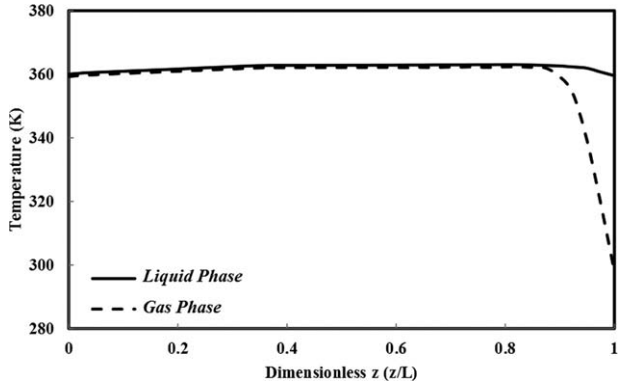

Figure 3. Temperature distribution along the reactor length.

Inlet liquid velocity = 0.0503 m/s, inlet gas velocity = 0.53 m/s, inlet gas pressure = 100 kPa, gas feed: 0.14 CO_2, MEA concentration = 1 M, wetting fraction = 0.1, inlet liquid temperature = 360 K, and inlet gas temperature = 298 K.

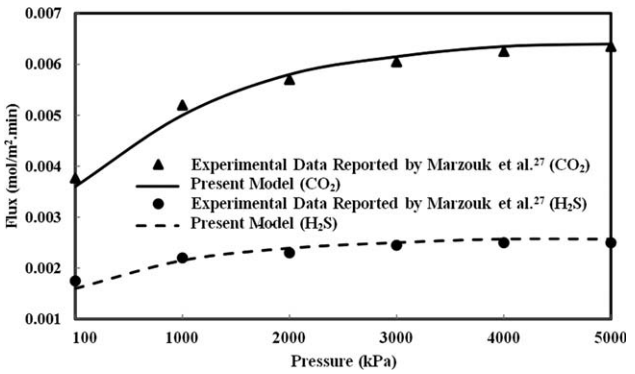

Figure 4. Comparison of simulation results with experimental data reported by Marzouk et al.[27] for the simultaneous absorption of CO_2 and H_2S using ePTFE-HFM.

MEA concentration = 0.5 M, gas flow rate = 1000 mL/min, and liquid flow rate = 25 mL/min.

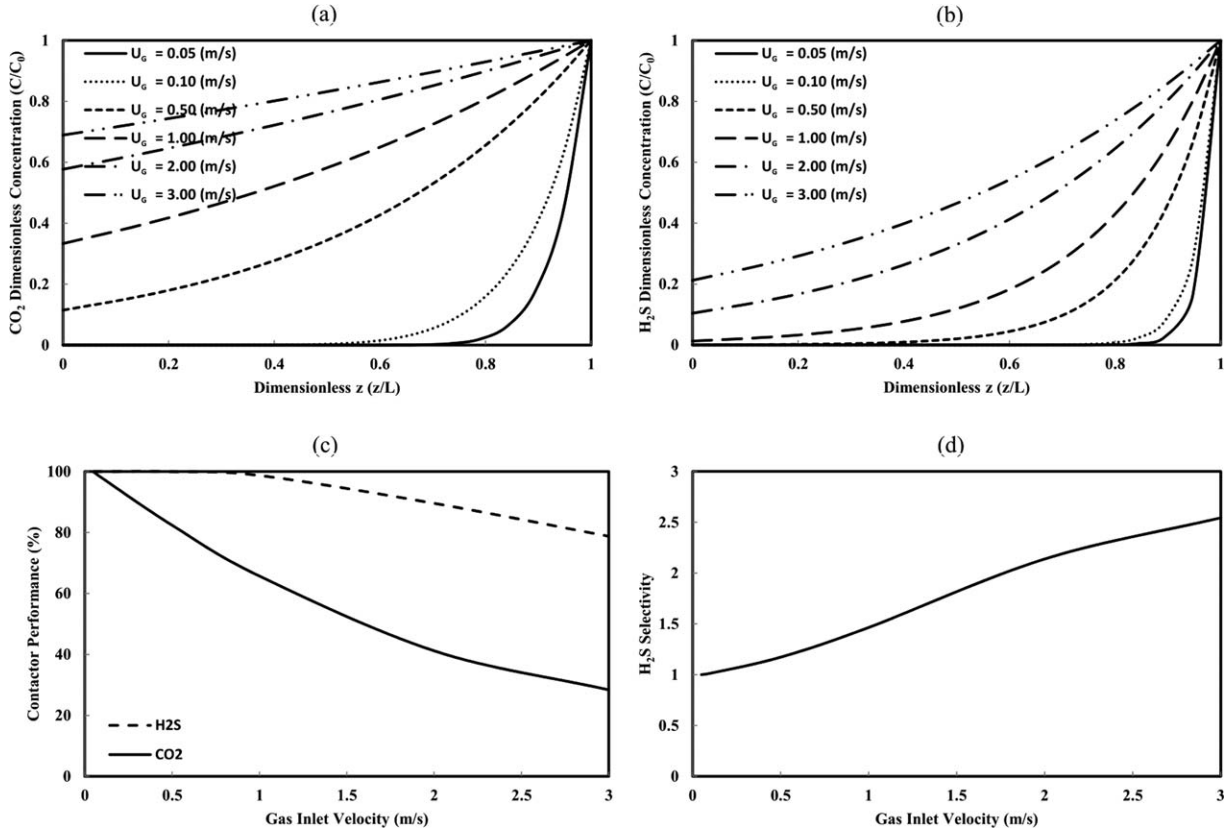

Figure 5. Effect of inlet gas velocity on the reactor performance.

Inlet liquid velocity = 1.0 m/s, inlet liquid temperature = 308 K, inlet gas pressure = 100 kPa, gas feed: 0.15 CO_2 and 0.05 H_2S, MEA concentration = 1.0 M, and wetting fraction = 0.1.

velocities. Moreover, due to large reaction rate constant of hydrogen sulfide, this effect is more significant for CO_2 than that for H_2S; therefore, with an increase in the inlet gas velocity, reactor selectivity for removing H_2S increases. In this regard, Figure 6 demonstrates the predictions of the present model without hydrogen sulfide in the gas-phase mixture against experimental data reported by Yan et al.[20] and as it is shown in this figure, excellent agreement was found.

Aqueous solution of MEA acts as a solvent in the reactor and as it is shown in Figure 7, larger velocities of the solvent provide better CO_2 and H_2S removal from the gas-phase mixture. Larger velocities of the solvent lead to larger MEA flow rates and, therefore, larger reaction rates of CO_2 and H_2S with MEA; hence, carbon dioxide and hydrogen sulfide concentration levels in the solvent phase decrease and as it may be obvious, with a decrease in CO_2 and H_2S concentrations in the solvent phase, driving force of mass-transfer rates increase. In other words, larger velocities of the solvent lead to lower residence time of removing components in the solvent phase and again it provides larger driving force for them to remove from the gas-phase mixture. Moreover, it has been found that the solvent bulk movement has more significant influence on the hydrogen sulfide removal compared to its influence on the removing CO_2. Again, the present model predictions are compatible with the available experimental data reported in the literature.[20]

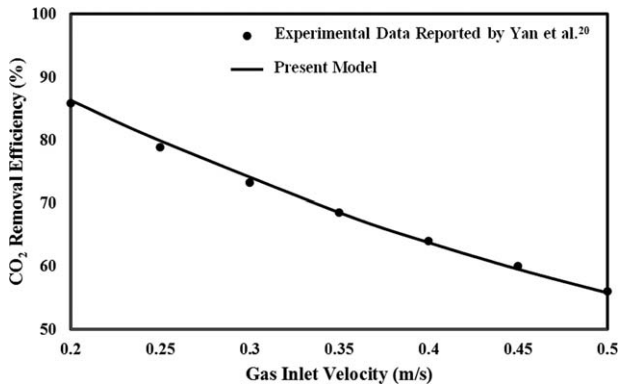

Figure 6. Validation of the model predictions against experimental data reported by Yan et al.[20]

Inlet liquid velocity = 0.0503 m/s, inlet liquid temperature = 308 K, inlet gas pressure = 100 kPa, gas feed: 0.14 CO_2, and MEA concentration = 1.0 M.

Figure 8 demonstrates the comparison of the predictions of present developed model with those of previous work presented by Al-Marzouqi et al.[28] (i.e., simpler model in the absence of H_2S). As it is shown in this figure, the present developed model considering the thermal energy equation, entrance region of momentum, heat, and mass transfers, the compressibility of the gas-phase mixture, physical solubility as a function of solvent temperature, solvent composition, and the gas pressure and, also, taking into account all molecular and convective terms of the governing equations offers significant advantage over simplified model. As it is shown in Figure 8, for small and large values of the solvent flow rate, the deviations of the previous developed models from the experimental data become significant. These obtained results for large values of the solvent flow rate can be

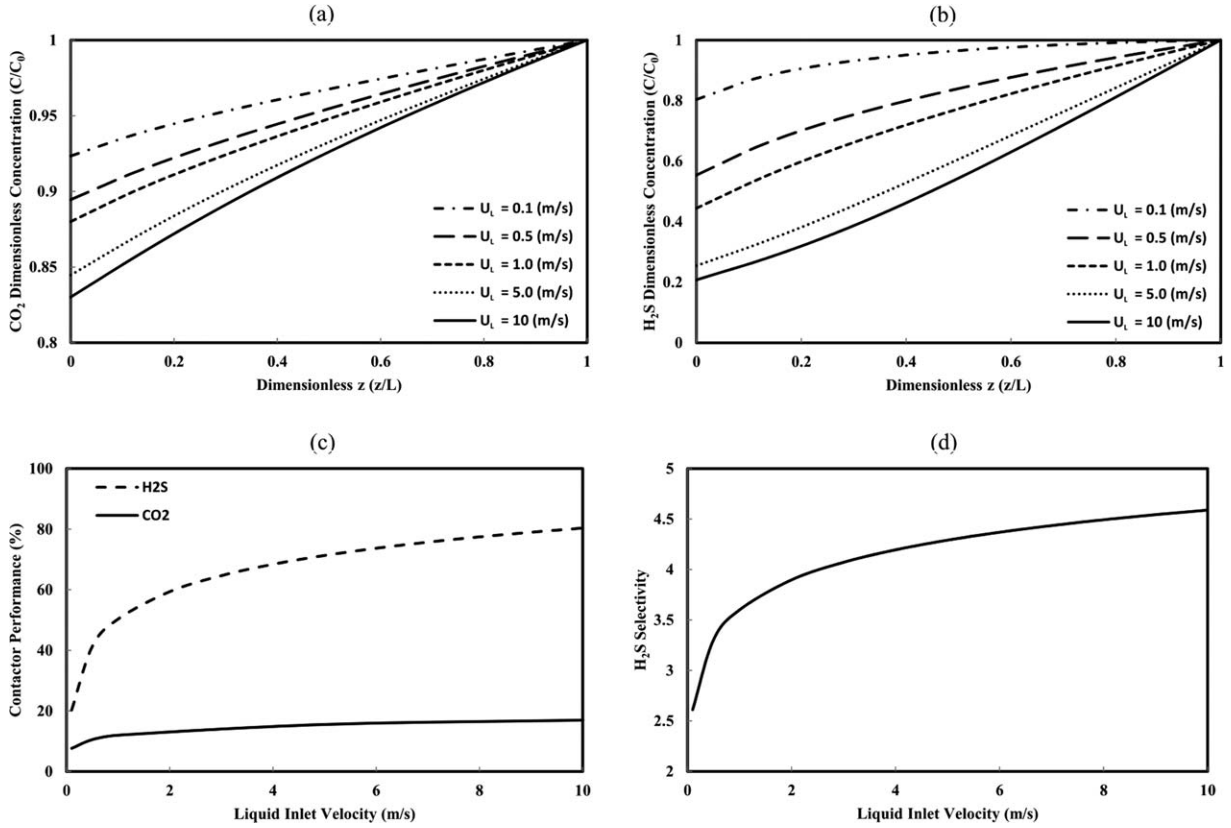

Figure 7. Effect of inlet solvent velocity on the reactor performance.

Inlet gas velocity = 2.0 m/s, inlet solvent temperature = 308 K, inlet gas pressure = 100 kPa, gas feed: 0.15 CO_2 and 0.05 H_2S, MEA concentration = 0.1 molar, and wetting fraction = 0.1.

explained by an increase in the entrance regions of the momentum, thermal energy, and mass transfers that can enhance the importance and necessity of their contributions in the prediction of the reactor performance. On the other hand, for small values of the solvent flow rates, the inevitable reduction of residence time of the solvent phase results in large temperature gradient in that phase. This is why the present developed model is so powerful in the prediction of appropriate data for both large and small values of the solvent flow rate.

Effects of the other important parameters on the steady-state behavior of the reactor are presented in Supporting Information, Appendix B.

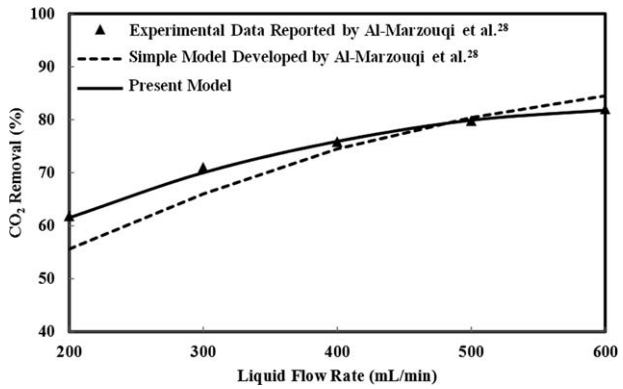

Figure 8. Comparison of the present model predictions with those of simplified models.

Inner tube diameter = 0.22 mm, outer tube diameter = 0.3 mm, shell diameter = 0.529 mm, module length = 0.2286 m, liquid temperature = 298 K, gas temperature = 298 K, CO_2 concentration = 4 mol/m^3, MEA concentration = 10 mol/m^3, gas flow rate = 600 mL/min, and pressure = 100 kPa.

Analysis of dynamic behavior of the reactor

To examine the effects of loads such as inlet gas velocity, inlet solvent velocity, feed gas, and MEA concentration of the solvent on the dynamic behavior of the membrane reactor, a number of simulation runs were performed. In this regard, Figures 9a, b demonstrate carbon dioxide and hydrogen sulfide concentrations variations in the shell side with time. Moreover, Figure 9c shows outlet CO_2 and H_2S concentration variations with time. As it is obvious from these figures, with increasing time, system reaches steady-state conditions and finally, some constant profiles in the shell side would be achieved. Moreover, Figure 9d shows the time variation of H_2S selectivity properly.

Figure 10 shows the effect of inlet gas velocity on the dynamic behavior of the reactor. As it may be expected; with an increase in the inlet gas velocity, the required time for achieving steady-state conditions decreases. However, for larger inlet gas velocities, there are larger carbon dioxide and hydrogen sulfide concentrations at the outlet of the reactor; thus, considering the initial condition of the simulations, there are two countereffect parameters leading to contrary observations illustrated in Figure 10.

Effects of the other important parameters on the dynamic behavior of the reactor are presented in Supporting Information, Appendix B.

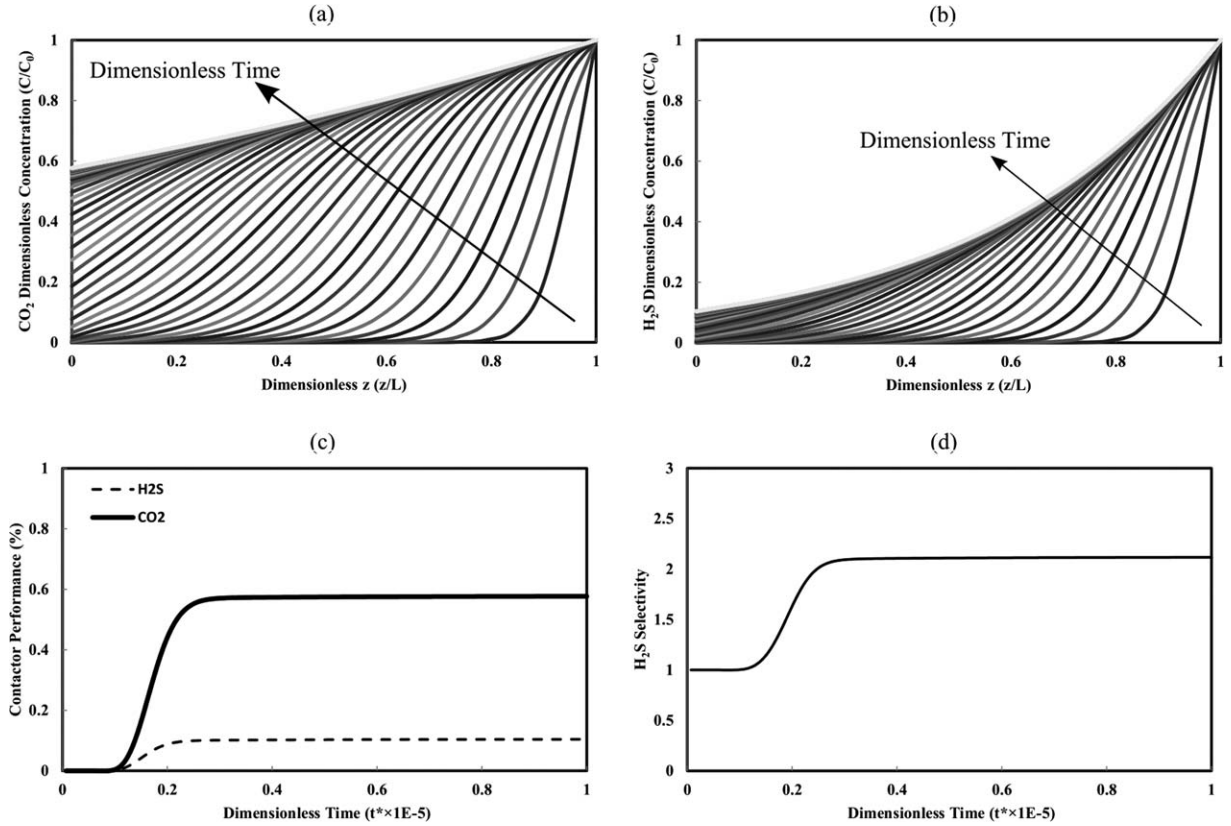

Figure 9. Dynamic behavior of the reactor performance.

Inlet liquid velocity = 1.0 m/s, inlet liquid temperature = 308 K, inlet gas pressure = 100 kPa, gas feed: 0.15 CO_2 and 0.05 H_2S, MEA concentration = 1.0 molar, wetting fraction = 0.1, and inlet gas velocity = 2.0 m/s.

Analysis of open-loop response of the reactor

To investigate the open-loop response of the reactor, we let the system to achieve steady-state conditions and then various types of step and pulse inputs were applied.

Step Changes. This section demonstrates the open-loop responses of the membrane reactor to some step changes on the contactor inlets. The reactor open-loop response varies from one steady-state operating point to another one and finally the time variations of CO_2 and H_2S outlet concentrations diminish. Moreover, these results clearly show excellent agreements with the obtained steady-state analysis. These analyses can nicely demonstrate the open-loop response of the membrane reactor to various step changes to the reactor inputs such as inlet gas velocity, inlet solvent velocity, feed gas concentration, and MEA concentration of the solvent.

As it is stated in the steady-state analysis section, smaller gas velocity, leads to larger removal of CO_2 and H_2S. Therefore, as shown in Figure 11, by applying a step decrease to the gas velocity, the system would be achieved a different steady-state operating point with an improved performance. To control the output concentration of CO_2 and H_2S during this step change (i.e., decreasing the gas velocity), it is possible to decrease the liquid velocity or decrease MEA concentration.

The open-loop dynamic response of the reactor applying step changes to the other important manipulated parameters are presented in Supporting Information, Appendix B.

Pulse Changes. To explore the dynamic response of the reactor to some pulse changes, four types of rectangular changes were applied to the reactor feed including carbon dioxide volume fraction and MEA concentration. Various pulse changes with duration equal to 5000 unit of the dimensionless time were applied to the mentioned system inputs as follows:

- Type 1. Negative pulse ($\Delta t^*=5000$).
- Type 2. Positive pulse ($\Delta t^*=5000$).
- Type 3. Negative pulse ($\Delta t^*=5000$) and subsequently positive pulse ($\Delta t^*=5000$).
- Type 3. Positive pulse ($\Delta t^*=5000$) and subsequently negative pulse ($\Delta t^*=5000$).

Tables 5 and 6 introduce the applied pulses to the solvent and feed gas, respectively. In all simulations, after each of these four pulse types, the system was achieved to its initial steady-state condition that means the reactor is dynamically stable.

Figures 12 and 13 show the open-loop response of the reactor to various pulse changes introduced to MEA concentration. Here, the reactor performance is decreased or increased for a while by applying negative and positive pulses, respectively. But, the time variations diminish after a while and the outlet conditions get back to their initial values. Moreover, as it is observed in Figure 13, negative-positive and positive-negative pulses (Types 3 and 4) show a sinusoidal time variations of the reactor performance.

Dynamic open-loop response of the contactor under applying various pulse changes on the feed gas composition are presented in Supporting Information, Appendix B.

Sinusoidal Gas Velocity. A simulation runs were performed to investigate the effect of sinusoidal inlet gas velocity on the time variations of the reactor performance (Figure

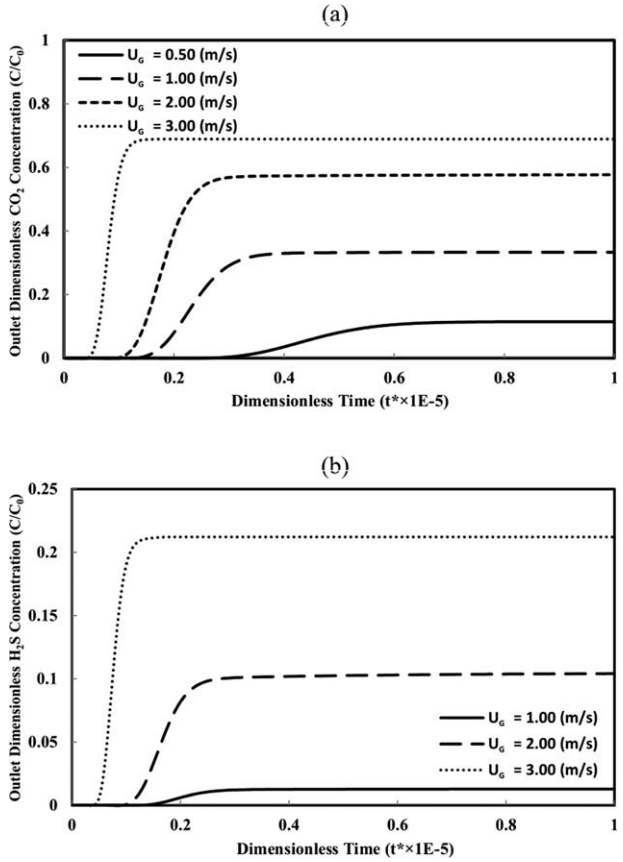

Figure 10. Effect of inlet gas velocity on the dynamic behavior of the reactor.

Inlet liquid velocity = 1.0 m/s, inlet liquid temperature = 308 K, inlet gas pressure = 100 kPa, gas feed: 0.15 CO_2 and 0.05 H_2S, MEA concentration = 1.0 molar, and wetting fraction = 0.1.

14). Consider sinusoidal inlet gas velocity with the following relation

$$U_{G_0}(t) = U \times (1 + A \times \sin(2\pi t/T)) \tag{88}$$

where U, A, and T are the time average velocity of the inlet gas, its amplitude, and period, respectively. At time equal to zero, this sinusoidal inlet gas velocity was applied to the reactor working at steady-state conditions with an inlet gas velocity of 1.0 m/s. As it may be expected, a sinusoidal time variation of the reactor performance is observed. After a while, the inlet gas velocity tends to its constant average value (1.0 m/s) and we let the system to achieve the steady-state condition; again, like the pulse change disturbances, as it is seen in Figure 14, the system turns back to its initial steady-state operating point.

Conclusions

In the present study, CFD techniques have been applied to analyze the transport phenomena in hollow fiber membrane reactors operated under nonwetted or partially wetted conditions. First goal of this work was to present a comprehensive model to obtain an accurate prediction of the experimental data considering the entrance regions of momentum, energy, and mass transfers, compressibility of the gas phase as a function of gas-phase temperature, pressure, and composition, and variation of physical solubility of CO_2 and H_2S as a function of gas-liquid interface temperature, pressure, and compositions. Taking into account the compressibility of the gas-phase mixture, make a significant advantage for the prediction of influence of inlet gas pressure. CFD methods have been applied to solve the nonlinear equations simultaneously, and the model predictions have been validated against available experimental data reported in the literature and excellent agreement has been obtained. By comparing the predictions of the present work with simplified models (in absence of hydrogen sulfide), it was found that the present model has significant advantages over other models. Moreover, for large or small values of the solvent flow rates, the developed model can properly predict the experimental data, whereas, the simplified models have deviations in their predictions. As the second goal of the present work, the dynamic behavior of the reactor and influences of some important input manipulated parameters on its dynamic behavior were studied carefully. Moreover, effects of various operating conditions (i.e., wetting fraction, gas and liquid inlet velocities, inlet pressure of the gas phase, MEA concentration, and CO_2 and H_2S volume fraction in feed gas) on the steady-state and transient distributions were studied and discussed. In third part of this work, we investigated the open-loop response of system by analyzing the system response to some step and pulse changes to the inlet conditions of gas (i.e., CO_2 and H_2S concentrations and velocity) or liquid (inlet liquid velocity and MEA concentration) phases. Results found can be expressed as:

Steady-state analysis

- It was found that temperature gradient in the liquid phase is not sharp and for the case study is around 3°C in the longitudinal direction. But, the gas-phase temperature varies to the liquid bulk temperature and, this is because of large Peclet number value of the liquid phase compared to its value for the gas phase. Therefore, for large gas velocities or small liquid velocities, the thermal energy equation can play an important role in the model predictions.
- With an increase in the inlet gas velocity, residence time of CO_2 and H_2S molecules in the reactor decrease; hence, reactor performance is reduced for both of them. But it is not a controlling parameter for the determination of H_2S removal and its effect is not significant compared with its effect on CO_2 removal; therefore, by increasing the gas inlet velocity, H_2S selectivity of the reactor increases.
- Larger CO_2 and H_2S concentrations in the feed have the same influence of increasing the inlet gas velocity and providing less reactor efficiency. Moreover, like the case of increasing the inlet gas velocity, larger values of both CO_2 and H_2S concentrations in the feed can lead to better hydrogen sulfide selectivity.
- Increasing MEA concentration in the inlet solvent results in larger reaction rate and therefore, more carbon dioxide and hydrogen sulfide removals would be achieved in the reactor. In addition, due to extremely large reaction rate constant value of hydrogen sulfide compared to its value for carbon dioxide, the influence of increasing MEA concentration on CO_2 removal is

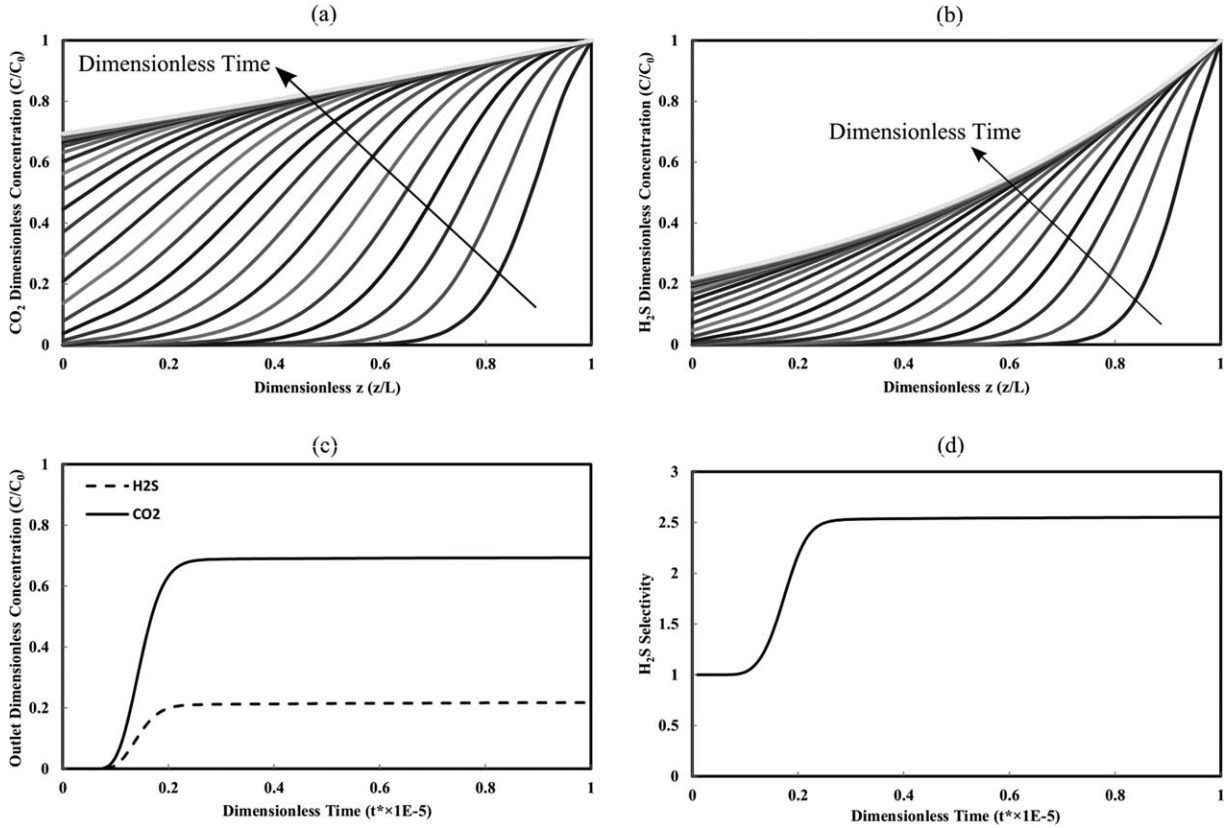

Figure 11. Steady-state response of the reactor affected by changing the inlet gas velocity from 0.05 m/s to 3.0 m/s.

Inlet liquid velocity = 1.0 m/s, inlet liquid temperature = 308 K, inlet gas pressure = 100 kPa, gas feed: 0.15 CO_2 and 0.05 H_2S, MEA concentration = 1.0 molar, and wetting fraction = 0.1.

more significant than that for H_2S; hence, by increasing the MEA concentration in the liquid phase, H_2S selectivity decreases.

- Larger velocities of the solvent provide larger bulk movement in the liquid phase and on the other hand, it causes to larger MEA concentration that leads to more reaction rate; so, there is larger driving force for carbon dioxide and hydrogen sulfide to be removed from the gas stream. Moreover, it was found that hydrogen sulfide is more sensitive to the liquid-phase bulk movement than CO_2; therefore, there are larger hydrogen sulfide selectivities for larger solvent velocities.
- For low wetting fractions, bulk movement of the liquid phase and MEA concentration level play an important role in the reduction of CO_2 and H_2S concentrations in the solvent consequently, increasing driving force of the mass transfer. Hence, by decreasing the wetted part of the membrane, convection of the liquid phase, and large concentration level of MEA can improve the reactor performance for both carbon dioxide and hydrogen sulfide. Moreover, it was found that by increasing the wetted part of the membrane, H_2S selectivity smoothly increases.

Table 5. Pulse Types Applied to the Solvent Phase

Solvent	Time	C_{MEA} (M)
• **Type 1**	$t^* < 0$	0.30
	$0 < t^* < 5000$	0.10
	$t^* > 5000$	0.30
• **Type 2**	$t^* < 0$	0.30
	$0 < t^* < 5000$	0.50
	$t^* > 5000$	0.30
• **Type 3**	$t^* < 0$	0.30
	$0 < t^* < 5000$	0.10
	$5000 < t^* < 10000$	0.50
	$t^* > 10000$	0.30
• **Type 4**	$t^* < 0$	0.30
	$0 < t^* < 5000$	0.50
	$5000 < t^* < 10000$	0.10
	$t^* > 10000$	0.30

Table 6. Pulse Types Applied to the Feed

Feed Gas	Time	Value (x_{CO2})
• **Type 1**	$t^* < 0$	0.20
	$0 < t^* < 5000$	0.05
	$t^* > 5000$	0.20
• **Type 2**	$t^* < 0$	0.20
	$0 < t^* < 5000$	0.35
	$t^* > 5000$	0.20
• **Type 3**	$t^* < 0$	0.20
	$0 < t^* < 5000$	0.05
	$5000 < t^* < 10000$	0.35
	$t^* > 10000$	0.20
• **Type 4**	$t^* < 0$	0.20
	$0 < t^* < 5000$	0.35
	$5000 < t^* < 10000$	0.05
	$t^* > 10000$	0.20

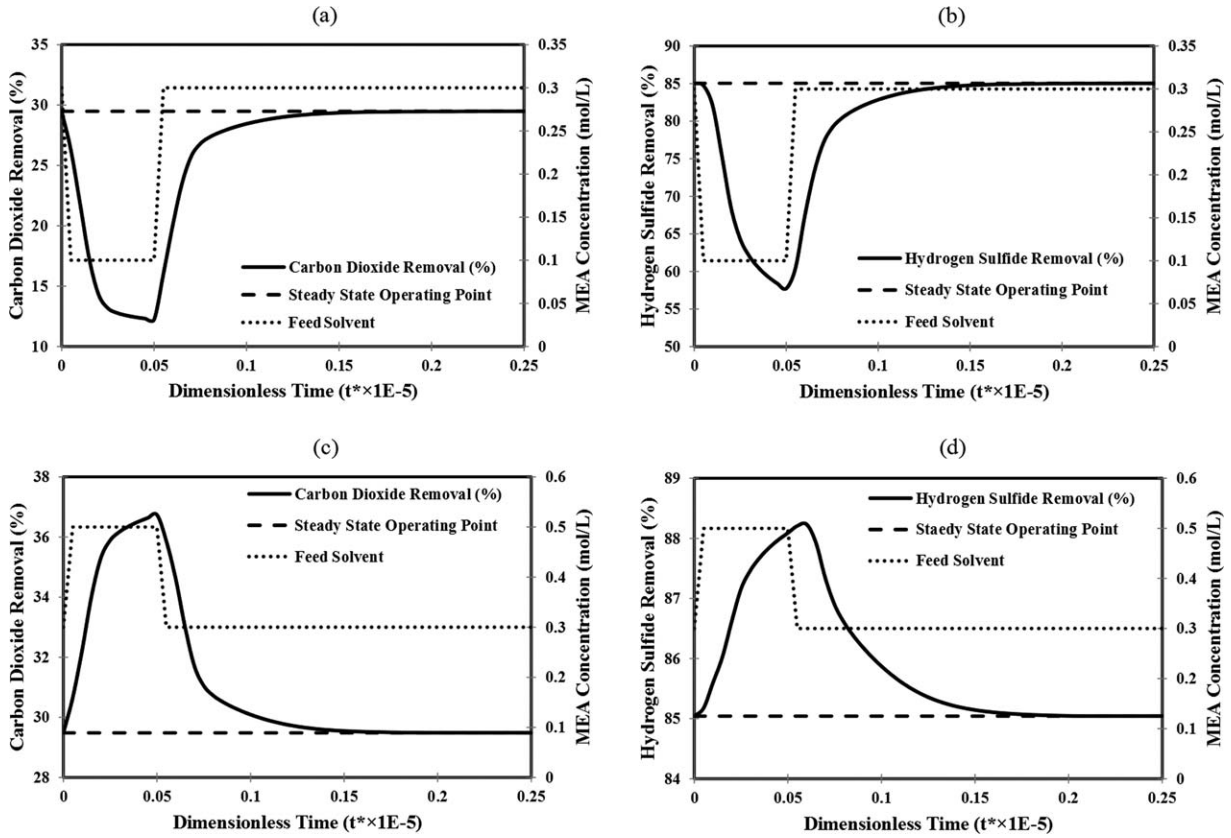

Figure 12. Open-loop response of the reactor under pulse change types 1 and 2 on the MEA volume fraction.

Inlet gas velocity = 2.0 m/s, inlet liquid velocity = 1.0 m/s, inlet liquid temperature = 308 K, inlet gas pressure = 100 kPa, gas feed: 0.15 CO_2 and 0.05 H_2S, and wetting fraction = 0.1.

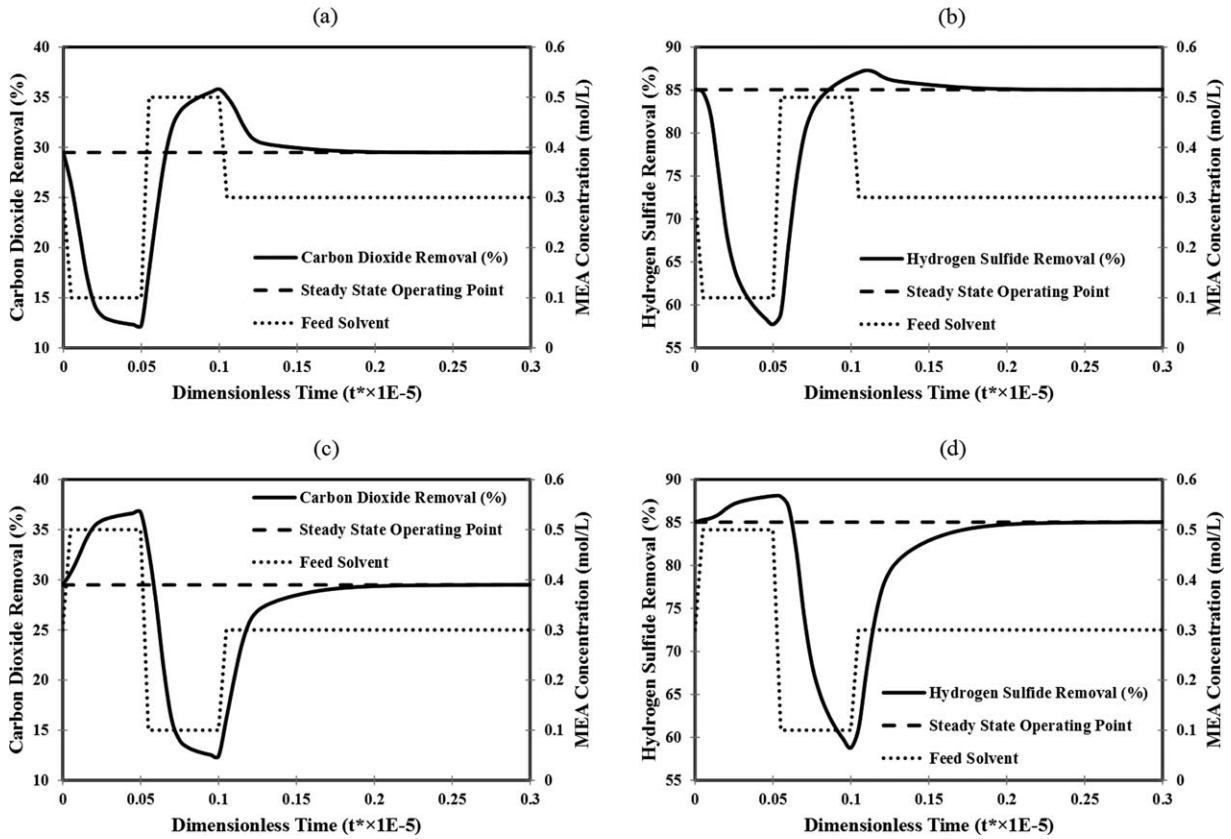

Figure 13. Open-loop response of the reactor under pulse change types 3 and 4 on the MEA volume fraction.

Inlet gas velocity = 2.0 m/s, inlet liquid velocity = 1.0 m/s, inlet liquid temperature = 308 K, inlet gas pressure = 100 kPa, gas feed: 0.15 CO_2 and 0.05 H_2S, and wetting fraction = 0.1.

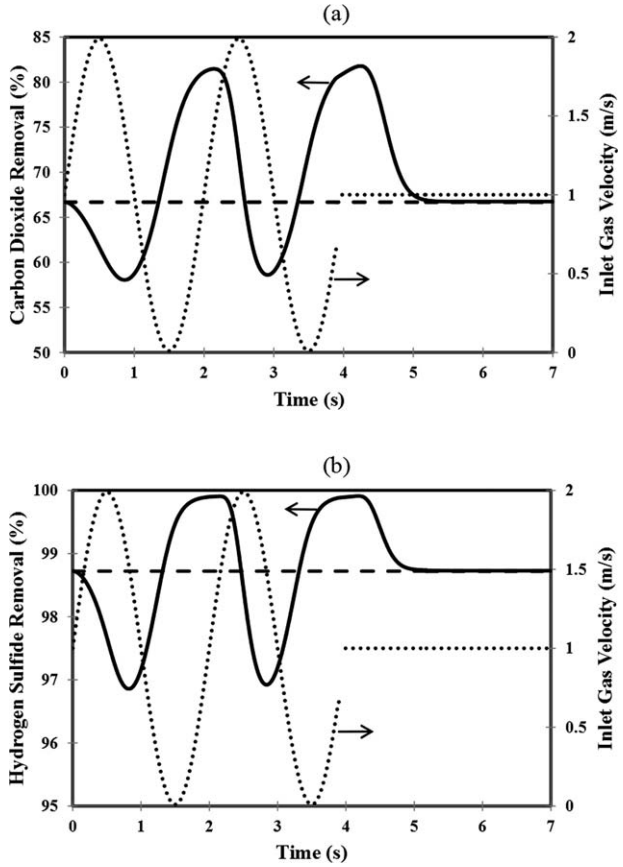

Figure 14. Open-loop response of the reactor to sinusoidal inlet gas velocity (Dash lines show the steady-state operating points).

Average inlet velocity = 1.0 m/s, inlet liquid velocity = 1.0 m/s, inlet liquid temperature = 308 K, inlet gas pressure = 100 kPa, MEA concentration = 1.0 molar, gas feed: 0.15 CO_2 and 0.05 H_2S, and wetting fraction = 0.1.

- It was found that all important parameter influencing the reactor behavior have more influence on CO_2 removal compared to H_2S; except the liquid bulk movement. Therefore, by increasing the liquid velocity which leads to significantly enhance the incorporation of the liquid bulk movement on CO_2 and H_2S removals, H_2S selectivity increases.

Transient analysis

- With an increase in the inlet gas velocity, residence time of the gas phase in the shell side decreases and also reactor performance is reduced. Considering the initial condition of simulations, these two effects have contrary influence on the required time for achieving steady-state conditions. But decreasing the gas-phase residence time is the major one and larger gas velocities lead to smaller required time for the reactor to attain steady-state profiles.
- Larger carbon dioxide and hydrogen sulfide concentrations in the system can provide larger reaction rates, therefore, smaller MEA concentration levels in the liquid phase. By decreasing MEA concentration, reaction rates of H_2S and CO_2 with MEA decrease; hence, increasing CO_2 and H_2S volume fractions in feed, increases the required time to achieve steady-state condition.
- Larger solvent velocities cause smaller residence time of the liquid phase in the tube side and better CO_2 and H_2S removals; hence, for larger inlet liquid velocities, smaller time is required for the process to attain the steady-state conditions.
- Decreasing the wetted part of the membrane affects the system performance by increasing the mass-transfer rate and driving force. Therefore, smaller wetting fraction leads to smaller steady-state required time.
- Larger MEA concentration in the solvent results in larger reaction rates and driving force for CO_2 and H_2S removals. So, by increasing the inlet MEA concentration, required time for achieving steady-state condition decreases.

Open–loop response analyses

- Using obtained results from the open-loop response of the reactor, it was found that the steady-state operating condition of the reactor does not depend on the initial condition and there is just one operating point for specified physical and operating conditions.
- Dynamic response of the reactor to various types of pulses on the feed and solvent shows that the system is dynamically stable and under various pulse changes gets back to its previous operating point.

Acknowledgment

The present author would like to thank Sharif University of Technology.

Notation

A = dimensionless number
Br = Brinkman number
C = concentration, mol m^{-3}
C_1 = constant
C_2 = constant, K
C_3 = constant
C_4 = constant, K^{-1}
C_p = specific heat capacity, kJ kg^{-1} K^{-1}
D = molecular diffusivity, m^2 s^{-1}
Da = Damkohler number
H = Henry's constant, kPa
k = thermal conductivity, kW m^{-1} K^{-1}
kr = kinetic rate constant, m^3 mol^{-1} s^{-1}
L = module length, m
m = modified Henry's constant, m^3 mol^{-1}
N = molar flux, mol m^2 s^{-1}
P = pressure, kPa
Pe = Peclet number
r = cylindrical coordinate, m
r_G = shell radius, m
r_L = tube radius, m
r_M = membrane radius, m
r_W = wetting radius, m
R = reaction rate, mol m^3 s^{-1}
Re = Reynolds number
T = temperature, K
V = velocity, m s^{-1}
x = liquid-phase mole fraction
y = gas-phase mole fraction
z = cylindrical coordinate, m

Greek letters

α = thermal diffusivity, m^2 s^{-1}
δ = heat capacity ratio, m^2 s^{-1}

ΔH = enthalpy change, kJ mol^{-1}
Δr = radial local step size, m
Δt = time step size, s
Δz = axial local step size, m
ε = membrane porosity
μ = viscosity, Pa s
v = kinematic viscosity, m^2 s^{-1}
ξ = dimensionless number
ρ = density, kg m^{-3}
σ = dimensionless number
τ = membrane tortuosity
Φ_v = viscous dissipation, s^{-2}

Subscripts

0 = entrance conditions
Ave = average
CO_2 = carbon dioxide
D = related to mass transfer
G = gas phase
GM = gas in membrane side
GS = gas in shell side
H = related to heat transfer
H_2O = water
H_2S = hydrogen sulfide
HS^- = sulfide
i = species index
ic = initial condition
j = species index
L = liquid phase
LM = liquid in membrane side
LT = liquid in tube side
mix = mixture
MEA = monoethanolamine
$MEAH^+$ = proton amine
$MEACOO^-$ = carbomate
r = r direction in cylindrical coordinate
R = reaction
s = solution
tot = Total
z = z direction in cylindrical coordinate

Superscript

$*$ = dimensionless number

Abbreviations

GM = gas in the membrane side
GS = gas in the shell side
LM = Liquid in the Membrane side
LT = Liquid in the Tube side

Literature Cited

1. Li JL, Chen BH. Review of CO_2 absorption using chemical solvents in hollow fiber membrane contactors. *Sep Purif Technol*. 2005;41:109–122.
2. Esato K, Eiseman B. Experimental evaluation of Core-Tex membrane oxygenator. *J Thorac*. 1975;69:690–697.
3. Qi Z, Cussler EL. Microporous hollow fibers for gas absorption, Part 1: mass transfer in the liquid. *J Membr Sci*. 1985;23:321–332.
4. Qi Z, Cussler EL. Microporous hollow fibers for gas absorption, Part 2: mass transfer across the membrane. *J Membr Sci*. 1985;23:333–345.
5. Feron PHM, Jensen AE. CO_2 separation with polyolefin membrane contactors and dedicated absorption liquids: performance and prospects. *Sep Purif Technol*. 2002;27:231–242.
6. Ren J, Wang R, Zhang HY, Li Z, Liang DT, Tay JH. Effect of PVDF dope rheology on the structure of hollow fiber membranes used for CO2 capture. *J Membr Sci*. 2006;281:334–344.
7. Kreulen H, Versteeg GF, Smolders CA, Van Swaaij WPM. Selective removal of H_2S from sour gas with microporous membranes, Part I: application in a gas-liquid system. *J Membr Sci*. 1992;73:293–304.
8. Wang D, Teo WK, Li K. Selective removal of trace H_2S from gas streams containing CO_2 using hollow fiber modules/contactors. *Sep Purif Technol*. 2004;35:125–13.
9. Boucif N, Favre E, Roizard D. Hollow fiber membrane contactor for hydrogen sulfide odor control. *AIChE J*. 2008;54:122–131.
10. Boucif N, Corriou JP, Roizard D, Favre E. Carbon dioxide absorption by Monoethanolamine in hollow fiber membrane contactors: a parametric investigation. *AIChE J*. 2012;58:2843–2855.
11. Coker DT, Freeman BD. Modeling multicomponent gas separation using hollow-fiber membrane contactors. *AIChE J*. 1998;44:1289–1302.
12. Faiz R, Al-Marzouqi M. Mathematical modeling for the simultaneous absorption of CO_2 and H_2S using MEA in hollow fiber membrane contactors. *J Membr Sci*. 2009;342:269–278.
13. Keshavarz P, Fathikalajahi J, Ayatollahi S. Mathematical modeling of the simultaneous absorption of carbon dioxide and hydrogen sulfide in a hollow fiber membrane contactor. *Sep Purif Technol*. 2008;63:145–155.
14. Wu B, Li K, Teo EK. Preparation and characterization of poly(vinylidene fluoride) hollow fiber membranes for vacuum membrane distillation. *J Appl Polym Sci*. 2007;106:1482–1495.
15. Taylor and Francis Group. *Handbook of Porous Media*, 2nd ed. CRC Press, Boca Raton, FL: CRC Press, 2005.
16. Vaidya PD, Kenig EY. CO_2-alkanolamine reaction kinetics: a review of recent studies. *Chem Eng Technol*. 2007;30:1467–1474.
17. Cornelissen AE. Simulation of absorption of H_2S and CO_2 into aqueous alkanolamines in tray and packed columns. *Trans Inst Chem Eng*. 1980;58:242–250.
18. Prausnitz JM, Lichtenthaler RN, de Azevedo EG. *Molecular Thermodynamics of Fluid-Phase Equilibria*, 3rd ed. Prentice Hall PTR, Inc., NJ: Prentice Hall PTR, 1999.
19. Smith JM, Van Ness HC, Abbott MM. *Introduction to Chemical Engineering Thermodynamics*, 7th ed. McGraw-Hill's Chemical Engineering Series, Boston, MA: McGraw-Hill's Chemical Engineering Series,, 2005.
20. Yan S, Fang M, Zhang W, Wang S, Xu Z, Luo Z, Cen K. Experimental study on the separation of CO_2 from flue gas using hollow fiber membrane contactors without wetting. *Fuel Process. Technol*. 2007;88:501–511.
21. Ashrae. *Ashrae Fundamentals Handbook*, SI ed. American Society of Heating, Refrigerating and Air-Conditioning Engineers, Inc., Atlanta, GA: American Society of Heating, Refrigerating and Air-Conditioning Engineers, Inc., 2009, 2009.
22. Akanksha, Pant KK, Srivastava VK. Carbon dioxide absorption into monoethanolamine in a continuous film contactor. *Chem Eng J*. 2007;133:229–237.
23. Polasek J, Bullin JA. Selecting amines for sweetening units. Technical Papers. Bryan Research and Engineering, Inc., Bryan, 1994.
24. Burgess MP, Germann RP. Physical properties of hydrogen sulfide-water mixtures. *AIChE J*. 1969;15:272–275.
25. Liu Y, Zhang L, Watanasiri S. Presenting vapor-liquid equilibrium for an aqueous MEA-CO_2 system using the electrolyte nonrandom-two-liquid model. *Ind Eng Chem Res*. 1999;38:2080–2090.
26. Hoffmann KA, Chiang ST. *Computational Fluid Dynamics*, 4rd ed., Wichita, KS: Engineering Education System Publication, 2000.
27. Marzouk S, Al-Marzouqi M, Teramoto M, Abdullatif N, Ismail Z. Simultaneous removal of CO_2 and H_2S from pressurized CO_2-H_2S-CH_4 gas mixture using hollow fiber membrane contactors. *Sep Purif Technol*. 2012;86:88–97.
28. Al-Marzouqi M, El-Naas M, Marzouk S, Abdullatif N. Modeling of chemical absorption of CO_2 in membrane contactors. *Sep Purif Technol*. 2008;62:499–506.

Manuscript received Mar. 28, 2013, and revision received Sept. 27, 2013.